V European Conference on Computational Fluid Dynamics
ECCOMAS CFD 2010
J. C. F. Pereira and A. Sequeira (Eds)
Lisbon, Portugal,14-17 June 2010

NUMERICAL SIMULATION OF DIRECTOR ORIENTATION OF NEMATIC LIQUID CRYSTAL IN TUMBLING FLOWS

Pedro A. Cruz*, **Murilo F. Tomé***

*Department of Applied Mathematics and Statistics
University of Sao Paulo,
Av. Trabalhador Saocarlense, 400, Sao Carlos, Sao Paulo, Brazil
e-mail: murilo@icmc.usp.br

Key words: Tumbling nematic liquid crystal, Ericksen-Leslie theory, Finite difference method, Liquid crystal, 2D flow

Abstract. *Liquid crystals have been studied and their applications are many, for example in display equipment electronics such as watches, computers and others. The use of liquid crystals results from the fact that intermolecular forces are easily affected by temperature, pressure and electromagnetic fields. The behavior of a molecule of nematic liquid crystal in a flow depends strongly on whether the nematic liquid crystal is of the tumbling or flow-aligning type. According to the Leslie-Ercksen theory, which assumes a nematic liquid crystal with a single director, tumbling behavior occurs when the ratio* $e = \alpha_3/\alpha_2$ *of the Leslie viscosities is positive. This means that the hydrodynamic torques force the director to process indefinitely in the flow. When* $e = \alpha_3/\alpha_2 < 0$*, the nematic liquid crystal becomes flow-aligned. This communication is concerned with the development of a numerical method for simulating director orientation of tumbling nematic liquid crystal for tumbling parameter* $e = 0.053$ *in channel flow subject to a finite magnetic field. The dynamic equations of nematic liquid crystals are based on the Ericksen-Leslie dynamic theory. The governing equations are solved by a finite difference technique based on the GENSMAC methodology [17, 19]. The resulting numerical method was verified by comparing the numerical solutions of 2D-channel flow throughout mesh refinement. To demonstrate the capabilities of the numerical method, the flow of a tumbling nematic liquid crystal was simulated using the "Ericksen-Leslie dynamic theory". Results are presented for various values of the Ericksen numbers.*

1 INTRODUCTION

Nematic liquid crystals are rather attractive owing to the applications in high performance optoelectronic products and their striking rheological properties. Nematic liquid crystals are characterized by long range orientational order of the molecules, in other words, the molecular orientation (alignment) in a nematic liquid crystal exhibits a preferred direction which can be represented by a unit vector $\mathbf{n}$, called the director.

The constitutive theory for liquid crystals started with the works of Anzelius [1] and Oseen [12] and culminated in the works of Leslie [9, 11] and Ericksen [5]. It has proven successful in describing many of the peculiar features of nematic liquid crystals behavior. This theory accounts for fluid anisotropy and elastic stresses resulting from spatial distortion of the director, and has commonly been used in analyzing flow behavior of nematic liquid crystals. The orientation of the director in flow of a nematic liquid crystal usually plays the most important role in their mechanical and optical properties. Thus, the study of the director orientation is the basis for many technological applications of nematic liquid crystals. The behavior of nematic liquid crystals in a flow is basically of two distinct kinds: *flow-aligned*, where the director is oriented at a fixed angle to the streamlines, and *tumbling*, where the hydrodynamic torques force the director to process indefinitely in the flow. Tumbling nematic liquid crystals are anisotropic, and the development of the anisotropic texture in processing geometries is a relatively-unexplored area of particular interest.

Several works investigating the flow of nematic liquid crystals exist in the literature (e.g. [2, 3, 7, 8, 14]). For instance, Heuer [7] studied the steady flow of nematic liquid crystals around an infinitely long cilinder, where, the director orientation was assumed to be parallel to the main flow direction. Cruz et. al. [3] developed a finite difference method for solving the dynamic Ericksen-Leslie equations in three-dimensions subject to a strong magnetic field. If the field is sufficiently strong then the director will be fixed: this means that the governing equation for the director may be neglected. To our knowledge, studies using the full Ericksen-Leslie equations for two-dimensional developing flows of tumbling nematic liquid crystals are extremely few.

In this paper we present a finite difference technique for solving the full Ericksen-Leslie dynamic equations in 2D channel for tumbling flows of a nematic liquid crystal.

2 GOVERNING EQUATIONS

We consider two-dimensional flow of a nematic liquid crystal. A magnetic field is applied and we assume the one-constant approximation for the elastic constants. The unitary director n_i and velocity v_i may take the forms

$$n_i = (\cos\phi, \sin\phi, 0), \qquad \phi = \phi(x, y, t), \tag{1}$$

$$v_i = (u(x, y, t), v(x, y, t), 0), \tag{2}$$

where ϕ is the orientation angle of the director. The magnetic field potential (equal to the negative of the magnetic energy) is

$$\Psi = \frac{1}{2}\mu_0 \Delta\chi (n_i \cdot H_i)^2, \quad \mathbf{H} = H(\cos\phi_0, \sin\phi_0, 0), \quad |\mathbf{H}| = H < \infty \tag{3}$$

where ϕ_0 =constant. The related external generalised body force G_i is given by

$$G_i = \frac{\partial \Psi}{\partial n_i} = \mu_0 \Delta\chi (n_i \cdot H_i) H_i \,, \tag{4}$$

where $\mu_0 > 0$ is the permability of free space and $\Delta\chi > 0$.

We shall use the usual Einstein summation convention where appropriate. A comma indicates partial differentiation with respect to the variable it precedes; for example $n_{i,j}$ denotes the partial derivative of the i^{th} component of n_i with respect to the j^{th} variable.

The basic equations for simulating two-dimensional flows of a nematic liquid crystal are the mass conservation equation, the elastic energy density, the linear and angular momentum equations which can be written, respectively, in dimensionless form as (for details see Cruz et al. [4])

$$u_{,x} + v_{,y} = 0 \,, \tag{5}$$

$$w_F = \frac{1}{2}\frac{1}{Re}\frac{1}{Er}\left[(\phi_{,x})^2 + (\phi_{,y})^2\right]. \tag{6}$$

$$u_t + uu_{,x} + vu_{,y} = -p_{,x} - w_{F,x} + R_j n_{j,x} + G_j n_{j,x} + \frac{1}{Re}\left(S_{xx,x} + S_{xy,y}\right), \tag{7}$$

$$v_t + uv_{,x} + vv_{,y} = -p_{,y} - w_{F,y} + R_j n_{j,y} + G_j n_{j,y} + \frac{1}{Re}\left(S_{yx,x} + S_{yy,y}\right), \tag{8}$$

$$\begin{aligned}\phi_t + u\phi_{,x} + v\phi_{,y} = {} & \frac{1}{Er\,\gamma_1}\left[\phi_{,xx} + \phi_{,yy}\right] - \frac{1}{2}(u_{,y} - v_{,x}) \\ & - \frac{1}{2}\frac{\gamma_2}{\gamma_1}\left[(u_{,y} + v_{,x})\cos(2\phi) + (v_{,y} - u_{,x})\sin(2\phi)\right] - \frac{1}{2}\frac{Re}{\gamma_1}\mu_0\Delta\chi H^2 \sin(2(\phi_0 - \phi))\end{aligned} \tag{9}$$

where $Re = \frac{\rho U L}{\eta}$ and $Er = UL\frac{\eta}{K}$ are the Reynolds and Ericksen numbers, respectively.

The terms $R_j n_{j,x}$, $R_j n_{j,y}$, $G_j n_{j,x}$ and $G_j n_{j,y}$ are given by

$$\begin{aligned} R_j n_{j,x} = {} & \frac{1}{Re}\{-\gamma_1\phi_{,x}\left[\phi_{,t} + u\phi_{,x} + v\phi_{,y} + \frac{1}{2}(u_{,y} - v_{,x})\right] \\ & -\frac{1}{2}\left[\gamma_2\phi_{,x}\cos(2\phi)(u_{,y} + v_{,x}) + \gamma_2\phi_{,x}\sin(2\phi)(u_{,x} - v_{,y})\right]\}, \end{aligned} \tag{10}$$

$$\begin{aligned} R_j n_{j,y} = {} & \frac{1}{Re}\{-\gamma_1\phi_{,y}\left[\phi_{,t} + u\phi_{,x} + v\phi_{,y} + \frac{1}{2}(u_{,y} - v_{,x})\right] \\ & -\frac{1}{2}\left[\gamma_2\phi_{,y}\cos(2\phi)(u_{,y} + v_{,x}) + \gamma_2\phi_{,y}\sin(2\phi)(u_{,x} - v_{,y})\right]\}, \end{aligned} \tag{11}$$

$$G_j n_{j,x} = \frac{1}{2}\mu_0 \Delta\chi H^2 \phi_{,x} \sin(2(\phi_0 - \phi)), \tag{12}$$

$$G_j n_{j,y} = \frac{1}{2}\mu_0 \Delta\chi H^2 \phi_{,y} \sin(2(\phi_0 - \phi)). \tag{13}$$

In the momentum equations (7) and (8) the components of the stress tensor S_{ij} are written as (see Cruz et al. [4])

$$S_{xx} = \frac{1}{Re}\left[2\, u_{,x} + \Phi^{xx}\right], \qquad S_{xy} = \frac{1}{Re}\left[\,(u_{,y} + v_{,x}) + \Phi_{xy}\right] \tag{14}$$

$$S_{yx} = \frac{1}{Re}\left[\,(u_{,y} + v_{,x}) + \Phi_{yx}\right], \qquad S_{yy} = \frac{1}{Re}\left[2\, v_{,y} + \Phi_{yy}\right]. \tag{15}$$

where the functions $\Phi_{xx}, \cdots, \Phi_{zz}$ are called non-Newtonian stress tensor, hereafter, are given by

$$\begin{aligned}
\Phi_{xx} &= \alpha_1 \cos^2\phi \left[u_{,x}\cos^2\phi + v_{,y}\sin^2\phi + \frac{1}{2}(u_{,y} + v_{,x})\sin(2\phi)\right] \\
&\quad - (\alpha_2 + \alpha_3)\sin\phi\cos\phi \left[\phi_t + u\phi_{,x} + v\phi_{,y} + \frac{1}{2}(u_{,y} - v_{,x})\right] \\
&\quad + (\alpha_5 + \alpha_6)\left[u_{,x}\cos^2\phi + \frac{1}{2}\sin\phi\cos\phi(u_{,y} + v_{,x})\right], \qquad (16) \\
\Phi_{xy} &= \alpha_1 \sin\phi\cos\phi \left[u_{,x}\cos^2\phi + v_{,y}\sin^2\phi + \frac{1}{2}(u_{,y} + v_{,x})\sin(2\phi)\right] \\
&\quad + (\alpha_3\cos^2\phi - \alpha_2\sin^2\phi)\left[\phi_t + u\phi_{,x} + v\phi_{,y} + \frac{1}{2}(u_{,y} - v_{,x})\right] \\
&\quad + \frac{1}{2}(\alpha_5\sin^2\phi + \alpha_6\cos^2\phi)(u_{,y} + v_{,x}) \\
&\quad + (\alpha_5 u_{,x} + \alpha_6 v_{,y})\sin\phi\cos\phi\,, \qquad (17) \\
\Phi_{yx} &= \alpha_1 \sin\phi\cos\phi \left[u_{,x}\cos^2\phi + v_{,y}\sin^2\phi + \frac{1}{2}(u_{,y} + v_{,x})\sin(2\phi)\right] \\
&\quad + (\alpha_2\cos^2\phi - \alpha_3\sin^2\phi)\left[\phi_t + u\phi_{,x} + v\phi_{,y} + \frac{1}{2}(u_{,y} - v_{,x})\right] \\
&\quad + \frac{1}{2}(\alpha_5\cos^2\phi + \alpha_6\sin^2\phi)(u_{,y} + v_{,x}) \\
&\quad + (\alpha_5 v_{,y} + \alpha_6 u_{,x})\sin\phi\cos\phi\,, \qquad (18) \\
\Phi_{yy} &= \alpha_1 \sin^2\phi \left[u_{,x}\cos^2\phi + v_{,y}\sin^2\phi + \frac{1}{2}(u_{,y} + v_{,x})\sin(2\phi)\right] \\
&\quad + (\alpha_2 + \alpha_3)\sin\phi\cos\phi \left[\phi_t + u\phi_{,x} + v\phi_{,y} + \frac{1}{2}(u_{,y} - v_{,x})\right] \\
&\quad + (\alpha_5 + \alpha_6)\left[v_{,y}\sin^2\phi + \frac{1}{2}\sin\phi\cos\phi(u_{,y} + v_{,x})\right]. \qquad (19)
\end{aligned}$$

In equations above, the viscosities $\alpha_1, \ldots, \alpha_6$ have been scaled by the factor η. Thus, the equations of motion (7) and (8) can be written in the form

$$\begin{aligned} u_t + uu_{,x} + vu_{,y} = -p_{,x} &- w_{F,x} + R_j n_{j,x} + G_j n_{j,x} \\ &+ \frac{1}{Re}\left[u_{,xx} + u_{,yy} + \Phi_{xx,x} + \Phi_{xy,y}\right], \qquad (20) \\ v_t + uv_{,x} + vv_{,y} = -p_{,y} &- w_{F,y} + R_j n_{j,y} + G_j n_{j,y} \\ &+ \frac{1}{Re}\left[v_{,xx} + v_{,yy} + \Phi_{yx,x} + \Phi_{yy,y}\right]. \qquad (21) \end{aligned}$$

Equations (5), (20), (21) and (9) form the complete set of dynamic equations and must be solved subject to suitable boundary conditions in order to find solutions for ϕ, p, u and v.

2.1 Boundary Conditions

In order to solve equations (5), (20), (21) and (9) it is necessary to impose boundary conditions for the velocity field on mesh boundaries. For rigid boundaries we employ the no-slip condition ($u_i = 0$) while at fluid entrances (inflows) the normal velocity is specified by $u_\nu = U_{inf}$ and the tangential velocities are set to zero, namely, $u_\mu = 0$, where ν denotes normal direction to the boundary and μ denotes tangential directions. At fluid exits (outflows) the Neumann condition $u_{i,\nu} = 0$ is adopted.

The director is strongly anchored on rigid boundaries (walls). In other words, the anchoring angle is set according to the orientation of the rigid boundary. Details of this anchoring angle will be given in the section dealing with the numerical results.

The choice of the angle of the director at fluid entrances (inflows) is $\phi = 0$, and at fluid exits (outflows) we set $\phi_{,\nu} = 0$.

3 NUMERICAL PROCEDURE

The momentum equations (20)-(21), the mass conservation equation (5) and the angular momentum equation (9) are solved by a methodology based on the GENSMAC algorithm introduced by Tomé et al. [19] as follows.

Assume that, at time t_n, the velocity field $u_i(x_k, t_n)$ and the orientation angle of the director $\phi(x_k, t_n)$ are known and that suitable boundary conditions are provided. In order to calculate the velocity field $u_i(x_k, t_{n+1})$, the pressure $p(x_k, t_{n+1})$ and the non-Newtonian tensor $\Phi_{ij}(x_k, t_{n+1})$, the orientation angle of the director $\phi(x_k, t_{n+1})$ we proceed in the following manner:

Step 1: Using the values of $u_i(x_k, t_n)$ and $\phi(x_k, t_n)$, solve Eq. (6) for $w_F(x_k, t_n)$ and calculate $\Phi_{ij}(x_k, t_n)$ from equations (16)-(19) and $R_j n_{j,i}(x_k, t_n), G_j n_{j,i}(x_k, t_n)$ using equations (10)-(13), respectively.

Step 2: Calculate a intermediate velocity field $\widetilde{u}_i(x_k, t_{n+1})$ by

$$\frac{\partial \widetilde{u}_i}{\partial t} = -(u_j\, u_i)_{,j} - w_{F,i} + R_j n_{j,i} + G_j n_{j,i} + \frac{1}{Re}\Big[\,(u_{i,j})_{,j} + \Phi_{ij,j}\Big] \tag{22}$$

with $\widetilde{u}_i(x_k, t_n) = u_i(x_k, t_n)$ using the same boundary conditions for the velocity $u_i(x_k, t_n)$. This equation is solved by an explicit finite difference method. It can be shown that $\widetilde{u}_i$ possesses the correct vorticity at time t_{n+1} (see Tomé et al. [18]).

Step 3: Solve the Poisson equation

$$\psi_{,ii}(x_k, t_{n+1}) = \widetilde{u}_{i,i}(x_k, t_{n+1}) \tag{23}$$

subject to the boundary conditions (see Tomé and McKee [17]): $\psi_{,\nu} = 0$ on rigid boundaries and inflows and $\psi = 0$ on outflows.

Step 4: Calculate the final velocity field

$$u_i(x_k, t_{n+1}) = \widetilde{u}_i(x_k, t_{n+1}) - \psi_{,i}(x_k, t_{n+1})\ . \tag{24}$$

Step 5: Determine the pressure field $p(x_k, t_{n+1})$ (see Tomé et al. [18])

$$p(x_k, t_{n+1}) = \frac{\psi(x_k, t_{n+1})}{\delta t}\ . \tag{25}$$

Step 6: Calculate the angle of the director $\phi(x_k, t_{n+1})$ from equation (9). This equation is solved by an explicit finite difference method.

Step 7: Calculate the components of the non-Newtonian tensor $\Phi_{ij}(x_k, t_{n+1})$ from equations (16)–(19).

4 FINITE DIFFERENCE APPROXIMATION

The equations contained in the numerical procedure outlined in the previous section will be solved by the finite difference method. A staggered grid is employed in this work. This was first introduced by Harlow and Welch [6] and it is commonly used with marker and cell methods because it locally guarantees conservation of mass and momentum while remaining computationally relatively simple.

For two-dimensional flows the velocities u and v are located at the faces of a cell while the variables (ϕ, Φ, p) are positioned at the centre of the cell. Figure 1 illustrates a typical two-dimensional cell of dimensions $\delta x \times \delta y$.

For this type of grid the components of the non-Newtonian tensor $\Phi_{i,j}$, the pressure p, the density of elastic energy (6) and the angular momentum equation (9) are calculated at the centre of the computational cell $(i\delta x, j\delta y)$ while the velocity components u and v are calculated at the faces $((i + \frac{1}{2})\delta x, j\delta y)$ and $(i\delta x, (j + \frac{1}{2})\delta y)$, respectively.

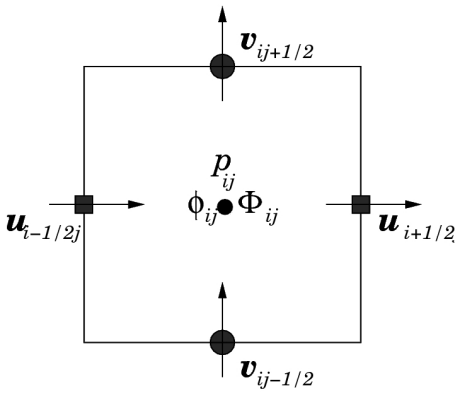

Figure 1: Typical two-dimensional staggered cell.

The time derivative in the momentum conservation equations (20)-(21) and in the angular momentum equation (9) are discretised by the explicit Euler method while the spatial derivatives are second order approximated. For lack of space, the finite difference equations involved will not be presented here; they can be found in Cruz et al. [4].

5 ADAPTIVE TIME-STEPPING

The explicit computation of the momentum equation can often result in a computationally inefficient code. To remedy this to some extent a time step is chosen, at each time point t_n, to be as large as possible while maintaining the stability of the scheme. Firstly, a particle of fluid, on each time step, cannot travel a distance greater than the spatial grid size. This implies the following restrictions

$$\delta t_x \leq \frac{\delta x}{|u|_{max}}, \tag{26}$$

$$\delta t_y \leq \frac{\delta y}{|v|_{max}}, \tag{27}$$

where $|u|_{max}$ and $|v|_{max}$ are the maximum modulus of the velocities in the directions x and y repectively.

The explicit discretisation of the momentum conservation equations also imposes a restriction on the stability. A von Neumann analysis of the equivalent linearised equation provides

$$\delta t_{visc} \leq \frac{Re}{2}\Big(\frac{1}{(\delta x)^2} + \frac{1}{(\delta y)^2}\Big)^{-1}. \tag{28}$$

The time step is chosen to be

$$\delta t = \min\{\delta t_x, \delta t_y, \delta t_{visc}\}.$$

The implementation of these restrictions to determine the allowable maximum temporal step is based on the ideas of Tomé and McKee [17].

6 VERIFICATION RESULTS

The numerical method presented in section 3 was implemented into a computer code to study two-dimensional flows and the spatial development of director orientation of tumbling nematic liquid crystals.

We simulated the flow of tumbling nematic liquid crystal 8CB (4-*n*-octyl-4'-cyano biphenyl) at 37°C. We considered a 2D-channel with width L and length $C = 10\,L$ (see figure 2). The boundary conditions for the velocity field were those specified in Sec. 2.1 . At the fluid entrance, a fully developed flow given by

$$u(y) = -4\frac{U}{L}\Big(y - \frac{L}{2}\Big)^2 + U \tag{29}$$

was imposed.

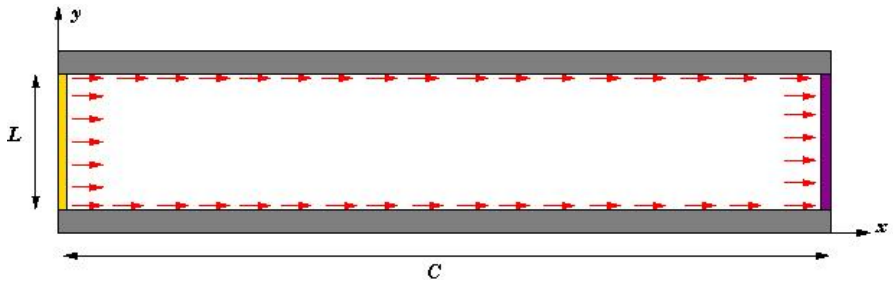

Figure 2: Definition of the domain for the simulation of the flow in a two-dimensional channel. The red arrows represent the boundary conditions used for the calculation of the angle ϕ by means of Eq. (9).

Boundary conditions for the angle ϕ

The boundary conditions for the angle ϕ were specified as follows:

1. Along the horizontal walls, the anchoring angle was set to zero, implying parallel alignment to the walls.

2. At the channel entry, we employed $\phi = 0°$ at $x = 0$ and $0 \leq y \leq L$ (see Fig. 2);

3. At the exit plane we assumed $\phi_{,x} = 0$.

To simulate this problem, the following input data specifying the flow were employed:

- Width of the entry of plane: $L = 0.001$m;
- Velocity scale: $U = 0.0001\,\mathrm{ms}^{-1}$;

The physical parameters, specifying the tumbling nematic liquid crystal 8CB at 37°C are given in Tables 1 and 2. With these data we obtain $Re = 0.015$ and $Er = 5$. To demonstrate the convergence of the numerical method presented in this paper, we simulated channel flow using four embedded meshes until steady state was achieved. The meshes employed were:

- M_0: $\delta x = \delta y = 0.0002$m ($50 \times 5$ cells)
- M_1: $\delta x = \delta y = 0.0001$m ($100 \times 10$ cells)
- M_2: $\delta x = \delta y = 0.00005$m ($200 \times 20$ cells)
- M_3: $\delta x = \delta y = 0.000025$m ($400 \times 40$ cells)

An analytic solution for this problem has not yet been found so that we compared the solutions obtained on meshes M_0, M_1 and M_2 to the solution obtained on the finer mesh M_3 which we refer here as *Exact*.

Figures 3 and 4 display the numerical and the *Exact* values of $u(y)$, Φ_{xx}, Φ_{xy}, Φ_{yx} and Φ_{yy} at the mid section of the channel ($x = 5$). We can see that there is a good agreement between the solutions. Moreover, Figs. 3 and 4 show that as the mesh is refined the numerical solutions tend to the *Exact* solution. These results suggest that the numerical method presented in this work is convergent.

To show quantitatively that convergence is achieved, the relative error of the numerical solution (Sol_{Num}) was calculated on the three meshes by the formula

$$E(\mathrm{Sol}_{Num}) = \sqrt{\frac{\sum\limits_{ij}(Exact - \mathrm{Sol}_{Num})^2}{\sum\limits_{ij} Exact^2}}. \tag{30}$$

The values of the relative errors obtained on the grids M_0, M_1 and M_2 are displayed in Table 3. It is noted in Table 3 that the errors decrease as the grid is refined which shows that the numerical method is convergent.

Table 1: Leslie viscosities for the tumbling nematic liquid crystal at 8CB given in SI units.

Leslie viscosities	α_1	α_2	α_3	α_4	α_5	α_6
8CB near 37°C	0.0000	-0.0588	0.0031	0.0140	0.0792	0.0235

7 NUMERICAL INVESTIGATION OF TUMBLING BEHAVIOR OF NEMATIC LIQUID CRYSTAL FLOW WITH THE TUMBLING PARAMETER ($e = 0.053$)

In this section we present numerical results from the simulation of the flow of a tumbling-type nematic liquid crystal in a two-dimensional channel (see Fig. 2). The

Table 2: Physical parameters for the tumbling nematic phases of 8CB given in SI units. The abbreviations used are: magnetic anisotropy ($\Delta\chi$ (unitless)) (see [15]), density (ρ) (see [15]), permeability of free space (μ_0), magnetic field (H) and elastic constant (K).

Phys. parameters	$\Delta\chi$	ρ	μ_0	H	K
Values	1.43×10^{-6}	1020 kg m^{-3}	12.566×10^{-7}H m^{-1}	$\frac{1}{4\pi}10^3$A m^{-1}	1.4×10^{-10} N

Table 3: Relative errors obtained on meshes M_0, M_1 and M_2.

Quantities	U	Φ_{xx}	Φ_{xy}	Φ_{yx}	Φ_{yy}
Rel. error (M_0)	9.7870×10^{-3}	3.5430×10^{-1}	8.4453×10^{-2}	4.2274×10^{-2}	1.8262×10^{-1}
Rel. error (M_1)	7.8150×10^{-3}	6.6565×10^{-2}	6.6950×10^{-3}	8.3780×10^{-3}	5.8730×10^{-2}
Rel. error (M_2)	2.7540×10^{-3}	2.0174×10^{-2}	2.3060×10^{-3}	3.0270×10^{-3}	1.8237×10^{-2}

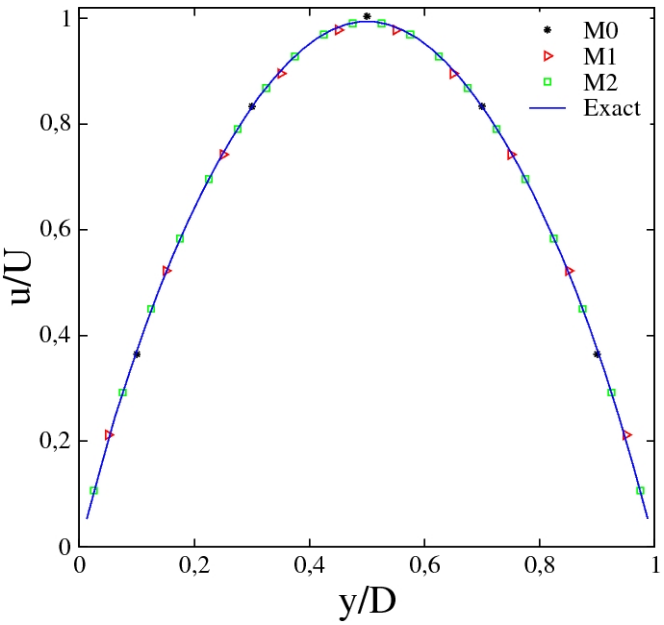

Figure 3: Numerical simulation of channel flow: $Re = 0.015$ and $Er = 5$. Comparison between the *Exact* and the numerical solutions at the $x = 5$. Velocity field.

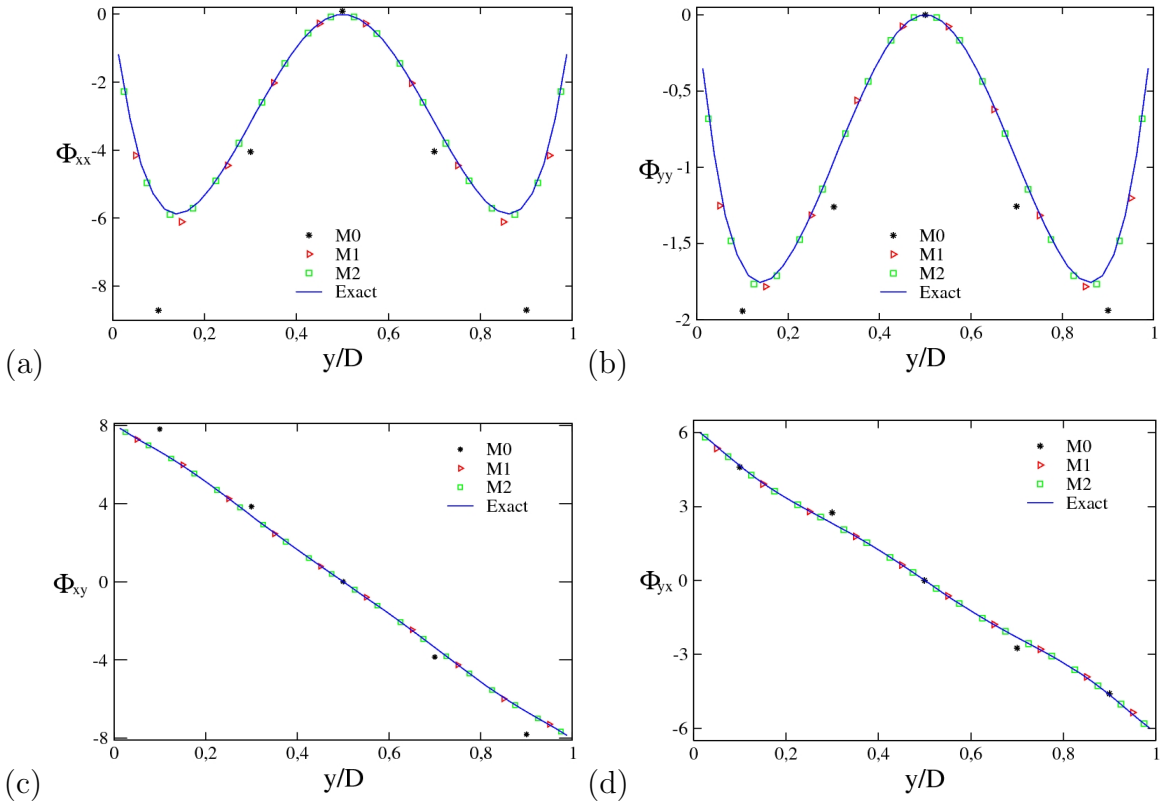

Figure 4: Numerical simulation of channel flow: $Re = 0.015$ and $Er = 5$. Comparison between the *Exact* and the numerical solutions at the $x = 5$. (a) Φ_{xx}, (b) Φ_{yy}, (c) Φ_{xy}, (d) Φ_{yx}.

boundary conditions employed on the inflow, channel walls and on the outflow were the same conditions used in the previous section.

The physical parameters specific to the tumbling nematic liquid crystal 8CB (4-*n*-octyl-4'-cyano biphenyl) at 37C° employed to simulate this problem are presented in Tables 1 and 2. The remaining input parameters were:

- Mesh: 200×20 cells $(\delta x = \delta y = 0.00005)$m;
- Width of the channel (length scale): $L = 0.001$m;
- Length of the channel: $C_1 = 0.01$m;
- Velocity scale: $U = 0.0001\,\mathrm{ms}^{-1}$;

The Reynolds and Ericksen numbers were calculated using the viscosity η so that we had $Re = 0.015$ and $Er = 5$. The behavior of a molecule of nematic liquid crystal in a flow depends strongly on whether the nematic liquid crystal is of the tumbling or flow-aligning type.

To observe the effects of elasticity, viscosity and the effects of the director orientation

on the flow, we simulated this problem until steady state was reached. We used channel with length $C_1 = 0.01$m: this distance was sufficient to reach the equilibrium angle of the development of director orientation. Channel flow was simulated for $Re = 0.015$, $e = 0.053$ and $Er = 1, 2, 3, \cdots, 100$ until $t = 200$. Figure 5 displays the isolines velocity u at time $t = 200$ for $Re = 0.015$ and $Er = 5$ with the boundary conditions for the director as specified in (see Fig. 2). We can see in Fig. 5 that the isolines of velocity u are parallel indicating that steady state has been reached.

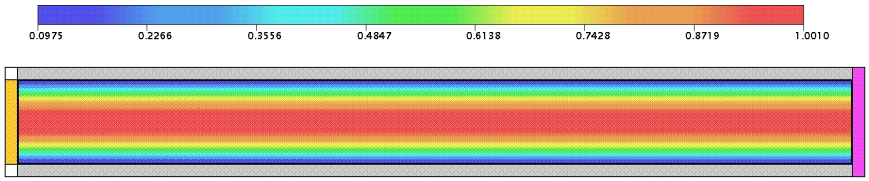

Figure 5: Numerical simulation of the flow of a tumbling-type nematic liquid crystal in a two-dimensional channel with $Re = 0.015$, $Er = 5$ and $e = 0.053$. Isolines of velocity u.

7.1 Maximum angle and spatial development orientation of director

We present the maximum orientation angle of the director in a fully-developed flow. The torque, due to viscosity of the nematic liquid crystal, that acts on the director induces rotation when $e > 0$. In the absence of a counter-torque the director would continue to rotate and an equilibrium orientation of the director could not be found.

The anchoring angle was set to zero along the walls, this condition induces an elastic torque because of director distortion, so there will be a maximum angle for developed flow inside the channel. In order to investigate the effect of the Ericksen number Er on the orientation angle of the director, the relation between the maximum orientation angle and Er obtained in the simulations when the Ericksen number was varied from 1 to 100 is shown in Fig. 6. We can see in Fig. 6 that the orientation angle of the director shows discontinuity at $Er \approx 5$ and $Er \approx 48$, with regions of possible multiplicity.

To study the two-dimensional spatial development of director orientation on the flow and to investigate the effect of this orientation on the velocity field, the evolution of the director orientation for $Er = 15, 40, 100$ is shown in Fig. 7 while the velocity profiles are shown in Figs. 8, 9, 10.

We can see in Fig. 7 that for $Er = 15$, the director rotated nearly 160° to reach the maximum angle shown in Fig. 6. The maximum angle of the director for $Er = 40$ is nearly 180°, and the development of the evolution of director orientation is similar to that for $Er = 15$, except that the position at which the director starts to rotate is shifted upstream. For $Er = 100$, the director rotated nearly 367° and the development of the evolution of director orientation starts to rotate further upstream. We can conclude that as we increased the Ericksen number the director profile became very complex in the

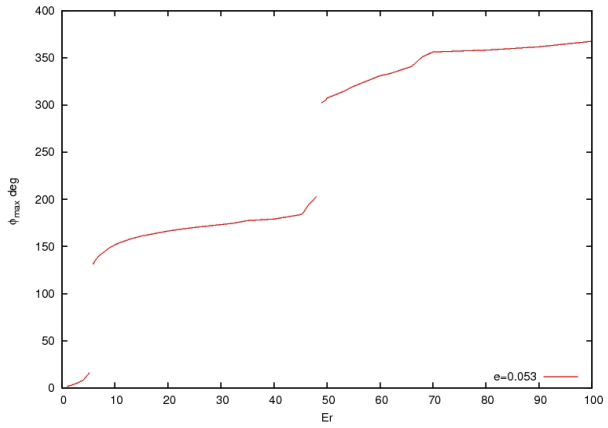

Figure 6: Maximum orientation angle of the director as a function of Ericksen number for fully-developed channel flow.

channel. Moreover, we can also see that there is a boundary layer that becomes thinner as the Ericksen number is increased.

The solutions obtained for the velocity field at selected points in the channel for Ericksen numbers $Er = 15, 40$ and 100 are shown in Figs. 8-10. We observe that the velocity profile u in the direction of the main flow becomes wavelike (Figs. 8 and 10). For $Er = 15$ we can observe the appearance of the vertical component of velocity v (see Fig. 9) near position $x = 2.05$. In this position the director begins to rotate in the flow as can be seen in Fig. 7(a). We can conclude that the effect the evolution of director orientation affected strongly the velocity field.

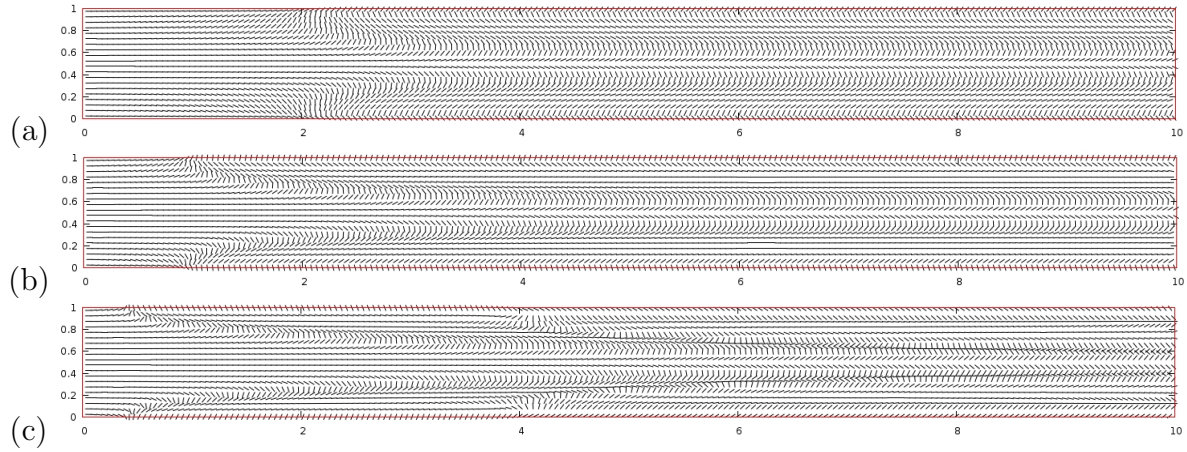

Figure 7: Spatial evolution of the director orientation between parallel plates with $e = 0.053$: a) $Er = 15$; (b)$Er = 40$; (c)$Er = 100$.

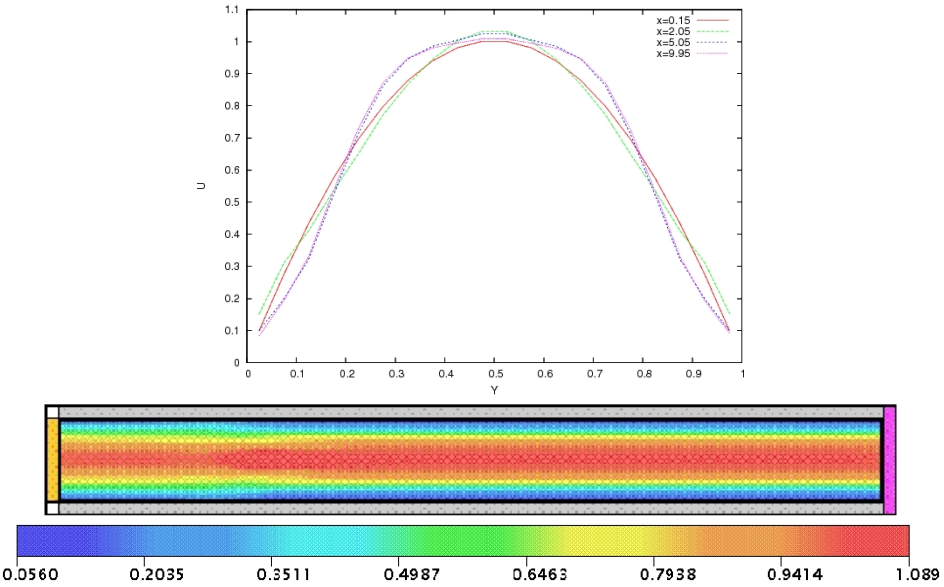

Figure 8: Velocity profiles u for $e = 0.053$ and $Er = 15$.

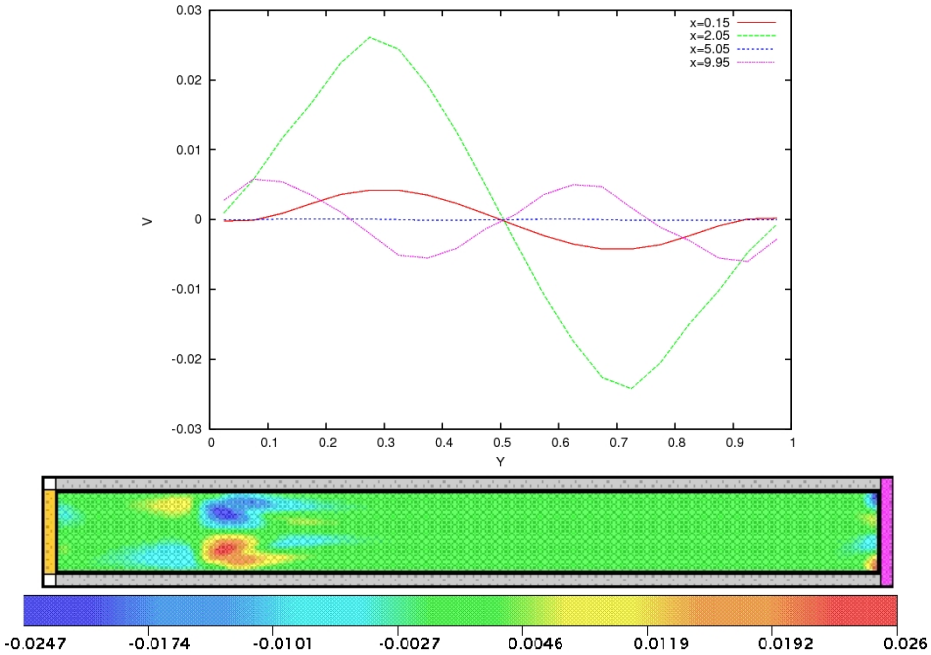

Figure 9: Velocity profiles v for $e = 0.053$ and $Er = 15$.

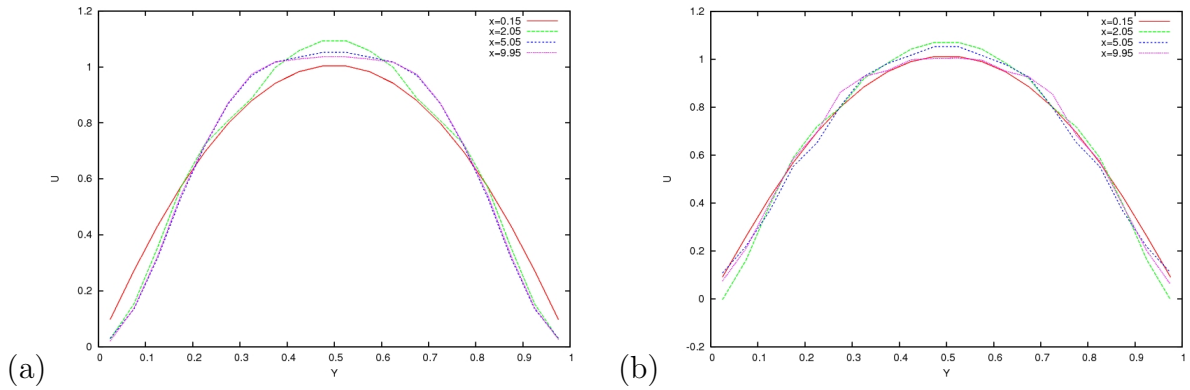

Figure 10: Velocity profiles u for $e = 0.053$ and $Er = 40$ (a) and 100 (b).

Figure 11 shows the behaviours of the orientation angle of director as a function of x, for $Er = 15, 40$ and 100, respectively. We can observe the transient behaviours of the orientation angle of the director. At $Er = 15$, there was a single rotation, and the maximum angle of the director was quickly reached. For $Er = 40$, the result is similar to that at $Er = 15$, except that the position at which the director started to rotate was shifted upstream, but the maximum angle of the director was rapidly reached. However, for $Er = 100$, the director presented a first rotation near the channel entrance ($x = 0.5$) and there was a second rotation nearly $x = 3.9$ before equilibrium was achieved.

Figure 12 displays the behaviours of the director angle profiles as a function of y, for $Er = 15, 40$ and 100, respectively. The maximum angle of the director was in the range $y \in [0.77, 0.87]$. The difference of the director angle between the upper wall and the centerline of the channel at position $x = 9.95$ and $y = 0.975$ was found to be approximately $51°$ when $Er = 15$, $71°$ for $Er = 40$ and $131°$ for $Er = 100$. Therefore, as the Ericksen number was increased the difference of the director angle between the upper wall and centerline of the channel also increased.

8 CONCLUSIONS

This paper employed the numerical method developed by Cruz et. al. [4] to investigate the director orientation of tumbling nematic liquid crystal in channel flow under the effect of a magnetic field. The verification of the method was performed through the simulation of the flow in a 2D channel using four embeeding meshes M0, M1, M2, M3. We compared the solutions on meshes M0, M1 and M2 to the solution obtained on the finer mesh M3 (which we called *Exact*). Good agreement between the solutions obtained on the coarser meshes and the *Exact* solution.

The flow in a 2D channel was simulated for the tumbling parameter $e = 0.053$ for Ericksen number varying between 1 and 100 and interesting effects were obtained. The results from the simulations showed that in a fully developed flow, the development of distribuition

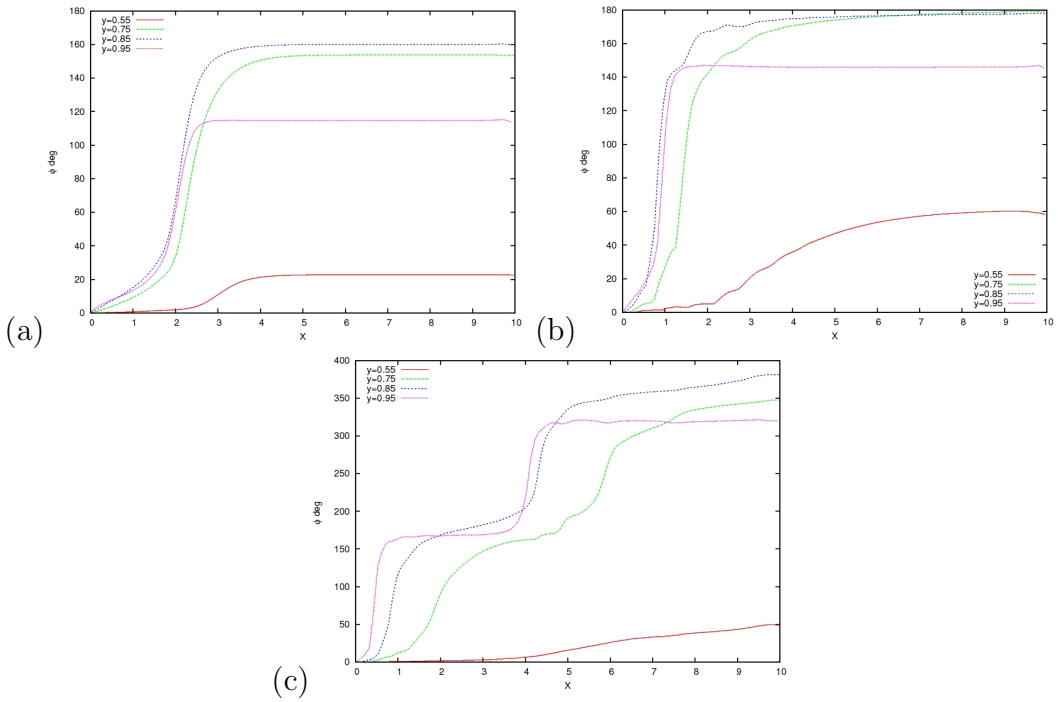

Figure 11: Orientation angle of the director at $y = 0.55, 0.75, 0.85$ and 0.95 as a function of x for $e = 0.053$ and: (a)$Er = 15$, (b) $Er = 40$ and (c) $Er = 100$.

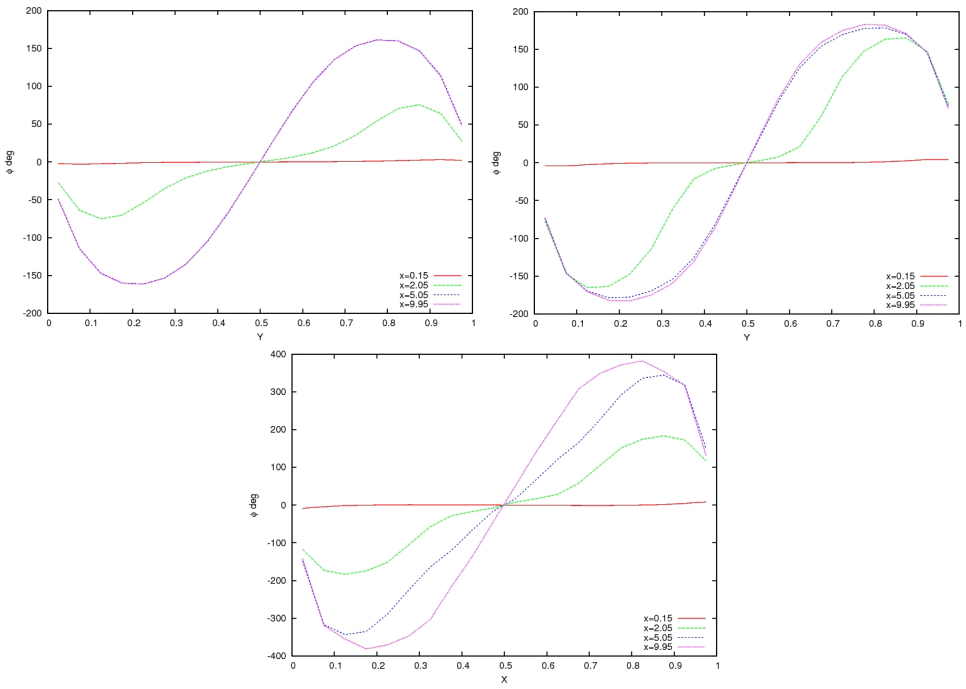

Figure 12: Orientation angle of the director at $x = 0.15, 2.05, 5.05$ and 9.95 as a function of y for $e = 0.053$: (a) $Er = 15$, (b) $Er = 40$ and (c) $Er = 100$.

director was governed by the number of director rotations necessary to reach the equilibrium angle. Another result was that, the maximum orientation angle of the director contains discontinuous jump between branches, with regions of possible multiplicity. The results also showed that the effect the evolution of director orientation affected strongly the velocity field. We observed that the velocity profile in the direction of the main flow became wavelike.

9 ACKNOWLEDGEMENTS

The authors would like to acknowledge the financial support given by the Brazilian funding agencies: FAPESP - Fundação de Amparo a pesquisa do Estado de São Paulo (grants 04/16064-9, 07/07038-2) and CNPq - Conselho Nacional de Desenvolvimento Científico e Tecnológico (grants Nos. 304422/2007-0, 470764/2007-4).

REFERENCES

[1] A. Anzelius, Bewegung der anisotropen Flüssigkeiten. Uppsala Univ. Årsskr, *Mat och-Naturvet.*, **1** (1931).

[2] S. Chono and T. Tsuji, Numerical simulation of nematic liquid crystalline flows around a circular cylinder. *Mol. Liq. Cryst.*, **309** (1998), 217–236.

[3] P. A. Cruz, M. F. Tomé, I. W. Stewart and S. McKee, A numerical method for solving the dynamic three-dimensional Ericksen-Leslie equations for nematic liquid crystals subject to a strong magnetic field.*J. Non-Newtonian Fluid Mech.*, **165** (2009), 143–157.

[4] P. A. Cruz, M. F. Tomé, I. W. Stewart and S. McKee, Numerical solution of the Ericksen-Leslie dynamic equations for two-dimensional nematic liquid crystal flows.*submitted J. Rheology* (2010).

[5] J.L. Ericksen, Conservation Laws for Liquid Crystals, *Trans. Soc. Rheol.*, **5** (1961), 23–34.

[6] F.H. Harlow and J.E. Welch. Numerical calculation of time-dependent viscous incompressible flow of fluid with free surface. *Phys. Fluids*, **8** (1965), 2182–2189.

[7] H. Heuer and H. Kneppe and F. Schneider, Flow of a Nematic Liquid Crystal Around a Cylinder, *Mol. Cryst. Liq. Cryst.*, **200** (1991), 51-70.

[8] J.T. Jenkins, Flows of Nematic Liquid Crystals, *Ann. Rev. Fluid Mech.*, **10** (1978), 197-219.

[9] F.M. Leslie, Some Constitutive Equations for Anisotropic Fluids, *Q. Jl. Mech. Appl. Math.* (1966), **19**, 357–370.

[10] F.M. Leslie, Some Constitutive Equations for Liquid Crystals, *Arch. Rat. Mech. Anal.* (1968), **28**, 265–283.

[11] F.M. Leslie, Theory of Flow Phenomena in Liquid Crystals, *Advances in Liquid Crystals*, **4** (1979), 1–81.

[12] C. W. Oseen. Beitäge zur Theorie der anisotropen Flüssigkeiten. *Arkiv För Matematik, Astronomi Och Fysik*, **19A**, part 9, 1–19, 1925.

[13] O. Parodi, Stress Tensor for a Nematic Liquid Crystal, *J. de Physique*, **31** (1970), 581–584.

[14] P. Pieranski and E. Guyon, Transverse Effects in Nematic Flows, *Physics Letters*, **49**A (1974), 237–238.

[15] M.J. Stephen and J.P. Straley, Physics of Liquid Crystals, *Reviews of Modern Physics*, **46** (1974), 617–704.

[16] I.W. Stewart, The Static and Dynamic Continuum Theory of Liquid Crystals, Taylor and Francis, London, 2004.

[17] M.F. Tomé and S. McKee. GENSMAC: A computational marker-and-cell method for free surface flows in general domains. *J. Comput. Phys.*, **110** (1994), 171–186.

[18] M.F. Tomé, B. Duffy and S. McKee, A Numerical Technique for Solving Unsteady Non-Newtonian Free Surface Flows, *J. Non-Newtonian Fluid Mech.*, **62** (1996), 9–34.

[19] M.F. Tomé, N. Mangiavacchi, J.A. Cuminato, A. Castelo and S. McKee, A finite difference technique for simulating unsteady viscoelastic free surface flows, *J. Non-Newtonian Fluid Mech.*, **106** (2002), 61–106.